

Article

Hydrochemical Appraisal and Driving Forces of Groundwater Quality and Potential Health Risks of Nitrate in Typical Agricultural Area of Southwestern China

Jiawei Liu ^{1,2} , Chang Yang ³ , Si Chen ³, Yangshuang Wang ^{1,2}, Xingjun Zhang ³, Wulue Kang ³, Junyi Li ³, Ying Wang ¹, Qili Hu ⁴ and Xingcheng Yuan ^{1,2,*}

¹ Yibin Research Institute, Southwest Jiaotong University, Yibin 644000, China

² Engineering Research Center of Groundwater Pollution Control and Remediation, Ministry of Education of China, Beijing Normal University, Beijing 100875, China

³ Observation and Research Station of Ecological Restoration for Chongqing Typical Mining Areas, Ministry of Natural Resources, Chongqing Institute of Geology and Mineral Resources, Chongqing 401120, China; cs9605@tom.com (S.C.)

⁴ State Environmental Protection Key Laboratory of Synergetic Control and Joint Remediation for Soil & Water Pollution, College of Ecology and Environment, Chengdu University of Technology, Chengdu 610059, China; huqili@cdut.edu.cn

* Correspondence: yxc123456@my.swjtu.edu.cn; Tel.: +86-182-2324-2939

Abstract: Elucidating the hydrogeochemical processes and quality assessment of groundwater holds significant importance for its sustainable development. In this paper, 53 groundwater samples were collected from a typical agricultural area in the northeastern Chongqing municipality in SW China. The integration of multivariate statistical analysis, ion ratio analysis, geomodelling analysis, the entropy water quality index, health risks assessment, and sensitivity analysis was carried out to explore the hydrochemical processes and quality assessment of groundwater in this study. The statistical results reveal that the cationic concentrations followed the order of $\text{Ca}^{2+} > \text{Mg}^{2+} > \text{Na}^+ > \text{K}^+$, while the anionic components were in the order of $\text{HCO}_3^- > \text{SO}_4^{2-} > \text{NO}_3^- > \text{Cl}^-$. Based on the Piper trilinear diagram, the hydrochemical types were shown as Ca-HCO₃ and Ca-Mg-HCO₃ types. Hierarchical cluster analysis indicated that the groundwater samples could be categorized into three groups. The hydrochemical compositions were primarily influenced by water–rock interactions (e.g., carbonate dissolution and silicate weathering). In terms of irrigation suitability, the sodium adsorption ratios (SARs) ranged from 0.05 to 1.82, and the electrical conductivity (EC) varied from 116 to 1094 $\mu\text{s}/\text{cm}$, indicating that most groundwater samples were suitable for irrigation. The entropy-weighted water quality index ranged from 15 to 94, suggesting that the groundwater samples were suitable for drinking purposes. Non-carcinogenic human health risks followed the order of children > adult females > adult males, within the average values of 0.30, 0.21, and 0.18, respectively. Sensitivity analysis showed that the parameters had the weight order of $\text{NO}_3^- > \text{body weight (BW)} > \text{ingestion rate (IR)} > \text{exposure frequency (EF)}$. Hence, we recommend prioritizing the management of areas with high salinity levels, while avoiding the excessive use of nitrogen fertilizers, raising awareness among local residents about safe groundwater, and providing robust support for the sustainable development of groundwater in typical agricultural areas.

Keywords: multivariate statistical analysis; water–rock interaction; groundwater quality; human health risk; sensitivity analysis; agricultural area



Citation: Liu, J.; Yang, C.; Chen, S.; Wang, Y.; Zhang, X.; Kang, W.; Li, J.; Wang, Y.; Hu, Q.; Yuan, X. Hydrochemical Appraisal and Driving Forces of Groundwater Quality and Potential Health Risks of Nitrate in Typical Agricultural Area of Southwestern China. *Water* **2023**, *15*, 4095. <https://doi.org/10.3390/w15234095>

Academic Editor: Dimitrios E. Alexakis

Received: 28 October 2023

Revised: 21 November 2023

Accepted: 22 November 2023

Published: 25 November 2023



Copyright: © 2023 by the authors. Licensee MDPI, Basel, Switzerland. This article is an open access article distributed under the terms and conditions of the Creative Commons Attribution (CC BY) license (<https://creativecommons.org/licenses/by/4.0/>).

1. Introduction

Groundwater is an indispensable natural resource, which serves as the primary cornerstone for human survival and societal progress [1]. It plays a crucial and irreplaceable function in facilitating economic expansion and preserving ecological balance [2]. The conflict

involving regional water supplies and groundwater environmental quality has emerged as a crucial development issue [3]. As the greatest developing nation internationally, the issue of China's water resource utilization deserves in-depth research. Groundwater accounts for 15.4% of the total water supply, but 77.3% of groundwater is deemed unsuitable for direct consumption [4,5]. In regions characterized by using nitrogen fertilizer in intense agricultural activity, nitrate contamination in groundwater often reaches elevated levels that pose a significant human health risk [6]. Prolonged ingestion of groundwater with elevated nitrate levels may lead to the development of diseases such as methemoglobinemia and gastric cancer [7,8]. Excessive agricultural activities contribute to an obvious deterioration in water quality, thereby posing a threat to drinking water safety for residents [9]. Meanwhile, timely monitoring of agricultural irrigation water quality stands as a vital measure in ensuring the efficient evolution of agricultural production [10].

The application of geography information systems (GISs) has become prevalent in the domain of groundwater monitoring and management [11]. The spatial distribution of hydrochemical parameters is indicated using a GIS [12]. Multivariate statistical analysis is a method that simultaneously examines and interprets the relationships between multiple variables, identifying primary correlations, trends, and variations within a dataset and providing valuable insights into the overall characteristics of groundwater systems [13]. Due to the numerous groundwater chemical parameters and their intricate interrelationships, along with the issue of inconsistent units among these parameters, directly discussing their multidimensional relationships becomes challenging. The principal component analysis (PCA) is a method used to simplify the complex relationships between various hydrochemical parameters, identify patterns of underlying trends, similarities, or differences in groundwater influenced by environmental factors, and aid in the assessment of interdependencies between arguments [14]. The objective of hierarchical cluster analysis (HCA) is to establish a methodology for classifying individual groundwater samples into distinct water quality categories, irrespective of factors such as the lithology of the aquifer, geological formations, and water-rock interactions [15]. Given that the inhabitants of the research area heavily rely on farming, coupled with the direct influence of groundwater quality on soil permeability and crop yield, appropriate hydrogeochemical parameters were selected to evaluate the applicability of agricultural irrigation purposes, such as the sodium adsorption ratio (SAR) and solute sodium percentage (%Na) [16]. The weighted water quality index (EWQI) surpasses the water quality index (WQI) by incorporating weighted factors, allowing for a more objective and comprehensive evaluation of groundwater quality that considers the relative importance of individual parameters [17]. The human health risk (HHR) model systematically assesses potential health risks linked to exposure to contaminated groundwater, considering factors such as contaminant concentrations, exposure pathways, and toxicity to estimate the likelihood and severity of adverse health effects on individuals exposed to the contaminated groundwater [18].

Northeastern Chongqing is a typical agricultural area with intense anthropogenic activity in southwestern China. Meanwhile, nitrate contamination has been identified in regional hydrogeological mapping, along with approximately 17% of groundwater samples exceeding the corresponding standard (20 mg/L). Nevertheless, groundwater quality assessment and the associated HHR in northeastern Chongqing have received relatively limited focus. Hence, it is imperative to enhance the knowledge of the groundwater's chemistry, quality, and health risks to ensure the sustainable management of groundwater resources in northeastern Chongqing. The primary objectives of this study were to (1) explore the hydrogeochemical characteristics of major ions in the groundwater, and (2) assess the potable and irrigation quality of the groundwater and potential human health risks. The findings of this study offer essential insights into the groundwater characteristics of northeastern Chongqing and give a vital reference for assessing water quality in an agricultural region.

2. Materials

2.1. Study Area

The study area is situated in the northeastern Chongqing municipality ($109^{\circ}45'20''$ – $109^{\circ}58'40''$ E and $31^{\circ}10'21''$ – $31^{\circ}19'52''$ N), where agriculture constitutes the primary economic industry (Figure 1). The climate is categorized as being of the mid-subtropical and sub-mountainous northern subtropical types. The annual average temperature and annual average rainfall are 18.4°C and 1049.3 mm. The terrain consists of low–middle mountains, low hills, and hilly plains [19]. In terms of land use types, the study region is characterized by agricultural land, which encompasses 46% of the total land area, with a focus on tobacco, corn, and wheat cultivation (Figure 1c). According to the data of the National Bureau of Statistics of China in 2019 [20], the amount of nitrogen fertilizer applied in Chongqing reached 441,000 tons, accounting for 48.4% of the total agricultural fertilizer; therefore, nitrogen fertilizer has been widely used.

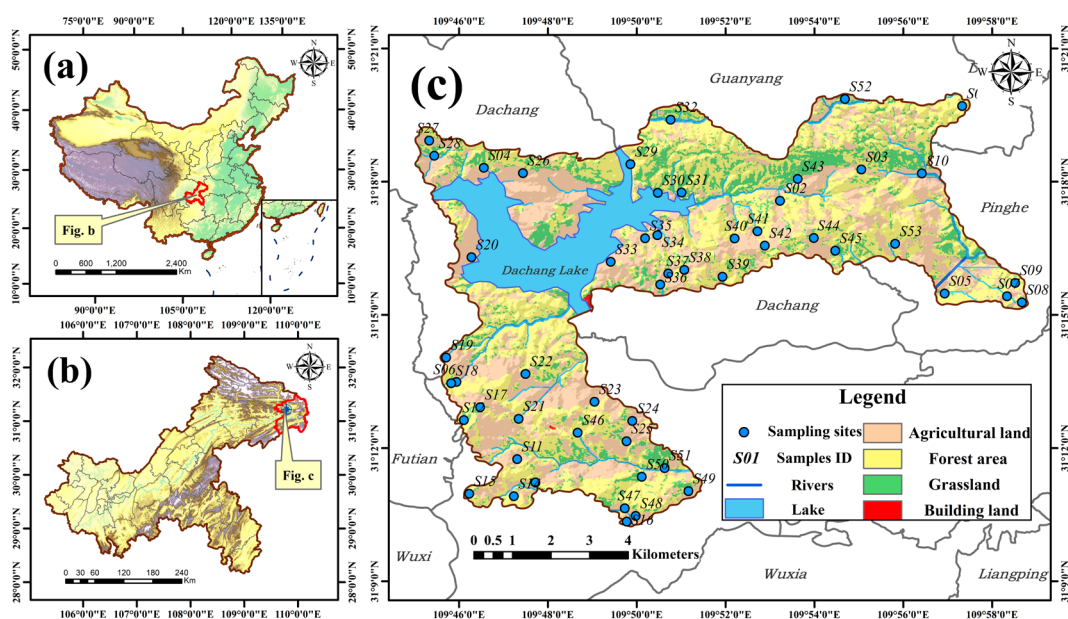


Figure 1. (a) Geographic location of Chongqing municipality in China. (b) The study area is located in the northeast of Chongqing municipality. (c) The distribution of groundwater sampling points and land use types in the study area, among which agricultural land occupies the largest proportion of 46%.

Geologically, the area is essentially located in the Daba Mountains. The strata consist of Triassic carbonate rocks (e.g., limestone and dolomite) and Permian clastic rocks (e.g., black shale, siliceous shale, interbedded gray-black thin–medium-bedded mudstone) [21,22]. Based on its hydrogeological characteristics, the groundwater is categorized into karst water (KW) in carbonate rocks and fissure water (FW) in clastic rocks [23,24]. KW is chiefly recharged via atmospheric precipitation, and surface water and is largely discharged in the form of springs. The flux in KW displays variation and ranges from 10 to $8640\text{ m}^3/\text{d}$. FW, similarly recharged in the form of atmospheric precipitation and surface water, also receives lateral recharge from KW. The primary discharge mechanism for FW is via springs, while some groundwater flows through linear seepage into surface water systems. The flux is relatively stable, ranging from 250 to $1500\text{ m}^3/\text{d}$.

2.2. Collection and Analysis of Groundwater Samples

In this paper, 53 groundwater samples were collected from different wells in January 2020 (Figure 1), and they were sent to the Chongqing Institute of Geology and Mineral Resources for experimental analysis in three days. The groundwater samples were all filtered

through a 0.45 μm filter and collected in sterilized plastic bottles (500 mL). Subsequently, all samples were hermetically sealed with parafilm, preserved in a 4 $^{\circ}\text{C}$ refrigerator and promptly transported for further experimental analysis.

The electrical conductivity (EC) and pH were determined using a portable multiparameter device (WTW-MultiLine Multi 3400i). The HCO_3^- concentration was determined using a Merck titration apparatus according to HNO_3^- . The remaining index testing methods were as follows: Na^+ , K^+ , Ca^{2+} , and Mg^{2+} concentrations were analyzed via ICP (ICP-OES) (Thermo Fisher ICAP-6300, Waltham, MA, USA); Cl^- , SO_4^{2-} , and NO_3^- concentrations were assessed using ion chromatography (ICS-2500, Dionex, Sunnyvale, CA, USA). The total dissolved solids (TDSs) were determined with the oven-drying method. The total hardness (TH) was titrated with EDTA-2Na.

The charge balance error (CBE) was utilized for accuracy confirmation (Equation (1)) [19]. The findings reveal that the CBE of major ions in the groundwater ranged from -2.7 to 5.4% , with an average of 1.4% .

$$CBE = \frac{\sum cations - \sum anions}{\sum cations + \sum anions} \times 100\% \quad (1)$$

3. Methods

3.1. Geochemical Modeling

Geochemical modeling with the PHREEQC (Version 3.3.9) program was utilized to determine the saturation indices (SIs) of minerals in the groundwater using Equation (2) [25]. When a mineral is in a supersaturated state, $SI > 0$; when a mineral is in an unsaturated state, $SI < 0$.

$$SI = \log\left(\frac{IAP}{K_{sp}}\right) \quad (2)$$

3.2. Assessment of Groundwater Quality

Currently, there are a great number of indicators available for evaluating the appropriateness of groundwater in agricultural irrigation activities [26]. In this paper, essential indexes (the sodium adsorption ratio and sodium percentage) for irrigation groundwater quality were identified to assess the groundwater's suitability in agricultural applications.

The SAR [27] is calculated as follows in Equation (3).

$$SAR = \frac{\text{Na}^+}{\sqrt{\frac{(\text{Ca}^{2+} + \text{Mg}^{2+})}{2}}} \quad (3)$$

The SAR index is commonly utilized for assessing the quality of irrigation groundwater. The ion exchange process occurring in water yields a reduction in soil permeability, thereby impeding nutrient absorption by crops and consequently impacting crop growth [16].

The %Na [28] is calculated as follows in Equation (4).

$$\%Na = \frac{\text{Na}^+ + \text{K}^+}{(\text{Ca}^{2+} + \text{Mg}^{2+} + \text{Na}^+ + \text{K}^+)} \times 100\% \quad (4)$$

Ion concentration units were measured in Meq/L , and the suitability of groundwater irrigation was evaluated by plotting USSL and Wilcox diagrams.

Compared with the traditional WQI index, the EWQI gives a more objective evaluation [29]. By incorporating information entropy into the quantitative assessment of water quality indicators, the method mitigates the influence of human subjectivity on data analysis, thereby promoting objective quantification [30]. The calculation steps of the EWQI are outlined below:

- (1) Determine the characteristic matrix X based on various parameters (Equation (5)).

$$X = (x_{ij})_{m \times n} = \begin{bmatrix} x_{11} & \cdots & x_{1n} \\ \vdots & \ddots & \vdots \\ x_{m1} & \cdots & x_{mn} \end{bmatrix} \tag{5}$$

- (2) In accordance with the natures of different parameters, determine the parameter types and normalize matrix X to derive the standardized matrix Y (Equations (6) and (7)).

$$y_{ij} = \begin{cases} \frac{x_{ij} - (x_{ij})_{\min}}{(x_{ij})_{\max} - (x_{ij})_{\min}} + 10^{-4} \text{benefit type} \\ \frac{(x_{ij})_{\max} - x_{ij}}{(x_{ij})_{\max} - (x_{ij})_{\min}} + 10^{-4} \text{cost type} \end{cases} \tag{6}$$

$$Y = (y_{ij})_{m \times n} = \begin{bmatrix} y_{11} & \cdots & y_{1n} \\ \vdots & \ddots & \vdots \\ y_{m1} & \cdots & y_{mn} \end{bmatrix} \tag{7}$$

- (3) Based on matrix Y, the information entropy (e_j) (Equations (8) and (9)) and entropy weight (w_j) (Equation (10)) are calculated.

$$P_{ij} = \frac{y_{ij}}{\sum_i^m y_{ij}} \tag{8}$$

$$e_j = -\frac{1}{\ln m} \sum_{i=1}^m (P_{ij} \times \ln P_{ij}) \tag{9}$$

$$w_j = \frac{1 - e_j}{\sum_{i=1}^n (1 - e_j)} \tag{10}$$

- (4) Determine the qualitative rating scale (q_i) (Equation (11)) for each variable and calculate the EWQI (Equation (13)), where the pH is calculated separately (Equation (12)).

$$q_i = \frac{C_j}{S_j} \times 100 \tag{11}$$

$$q_{\text{pH}} = \frac{\text{pH} - 7}{S_{\text{pH}} - 7} \times 100 \tag{12}$$

$$\text{EWQI} = \sum_{j=1}^m (w_j \times q_j) \tag{13}$$

where m is the number of water samples, n is the evaluated hydrochemical indicator; P_{ij} is the j th parameter value of sample i ; q_j is the quantitative rating scale of the hydrochemical parameter classification, calculated from the concentration C_j of hydrochemical parameter j ; and S_j is the permissible limit from the Chinese standard for groundwater quality [31] for parameter j . The EWQI levels are clarified based on Table S1 [32].

3.3. Human Health Risk Assessment

Previous research has shown that the human health risk is mostly linked to the oral intake of groundwater [33]. Considering the concentrated nitrate concentration in the study area, this paper predominantly focused on evaluating the human non-carcinogenic health risks linked to oral intake [34]. The main parameters for the HHR model are presented in Table S2.

- (1) The chronic daily intake (CDI) of contaminated groundwater ingested directly was calculated based on various physicochemical parameters [35] (Equation (14)).

$$CDI = \frac{CW \times IR \times EF \times ED}{BW \times AT} \quad (14)$$

where BW is the average body weight; AT represents the average exposure time; CW is the groundwater contaminant concentration; IR is the daily oral ingestion rate; EF indicates the exposure frequency; and ED denotes the exposure duration.

- (2) The human health hazard quotient (HQ_i) of contaminated groundwater is determined by utilizing Equation (15).

$$HQ_i = \frac{CDI}{RfD_i} \quad (15)$$

where RfD_i represents the reference dose.

The hazard index (HI) is calculated as follows in Equation (16).

$$HI = HQ_1 + HQ_2 + \dots + HQ_i \quad (16)$$

An HQ or HI of > 1 indicates pollutants may exist that pose potential harm to human health. On the contrary, if the HQ or HI is < 1 , there are no hazards.

4. Results

4.1. Spatial Characteristics of Hydrochemistry

The spatial characteristics of hydrochemistry are displayed in Figure 2. The concentration of K^+ was relatively limited and prevalently dispersed in the southeastern area. Na^+ and Cl^- were predominantly concentrated in the southwest and eastern regions, indicating the possibility of a similar source. Ca^{2+} and HCO_3^- were predominantly distributed in the eastern and northwestern regions. Their extensive distribution and higher concentrations demonstrated that Ca^{2+} and HCO_3^- were the major controlling ions within the study area and originated from the same source. Mg^{2+} was primarily located in the southwestern, central, and eastern areas. SO_4^{2-} was concentrated in the southwestern region. The limited distribution characteristics and considerable differences in concentration expressed that sulfides within local coal-bearing seams may have exerted an impact on the concentration of SO_4^{2-} . The presence of NO_3^- serves as a toxicological indicator for human health in groundwater, and prolonged consumption of high levels of NO_3^- in groundwater might lead to severe harm to humans [36]. The NO_3^- was primarily in the southwest and east regions, suggesting that groundwater management should be significantly concentrated in those regions.

4.2. Hydrochemical Facies

Based on various hydrochemical parameters of groundwater samples, hierarchical cluster analysis (HCA) can be applied for hydrochemical classification [37]. The samples were associated and grouped using the average Euclidean distance, and a pedigree dendrogram was drawn using hierarchical cluster analysis [38,39]. Three groups (G1, G2, and G3) of 53 groundwater samples were recognized (Figure 3). The statistical analysis of hydrogeochemical components constitutes a general analytical method for characterizing the chemical composition of groundwater [40]. In this paper, box plots depict the basic characteristics of the groundwater chemical parameters (Figure 4; Table 1).

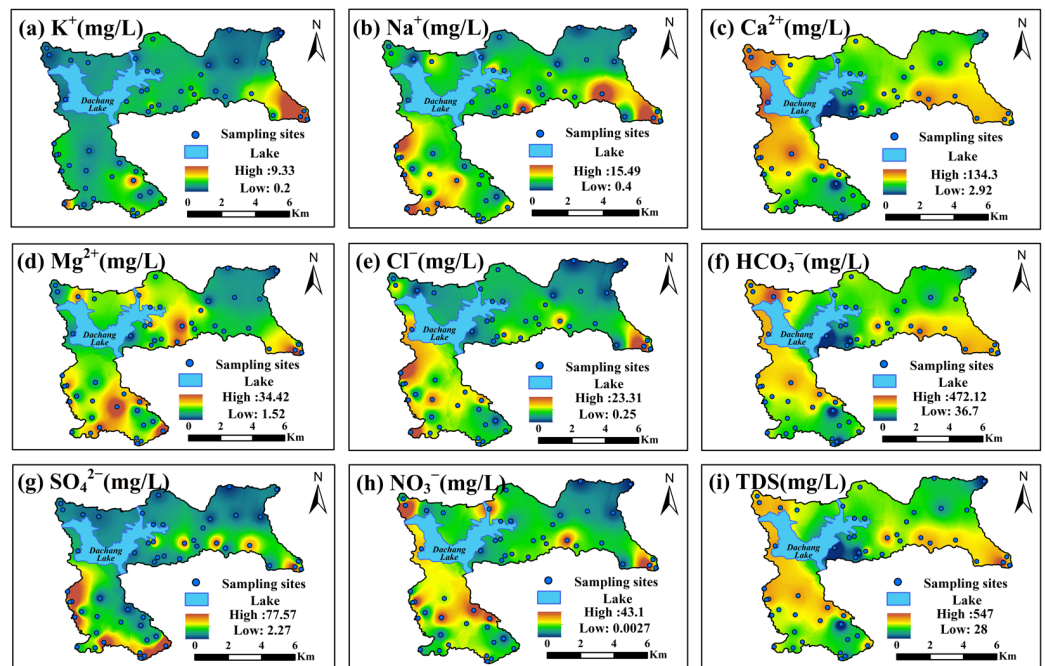


Figure 2. Distribution characteristics of different hydrochemical indicators in northeastern Chongqing municipality, China. (a) K^+ , (b) Na^+ , (c) Ca^{2+} , (d) Mg^{2+} , (e) Cl^- , (f) HCO_3^- , (g) SO_4^{2-} , (h) NO_3^- , and (i) TDS.

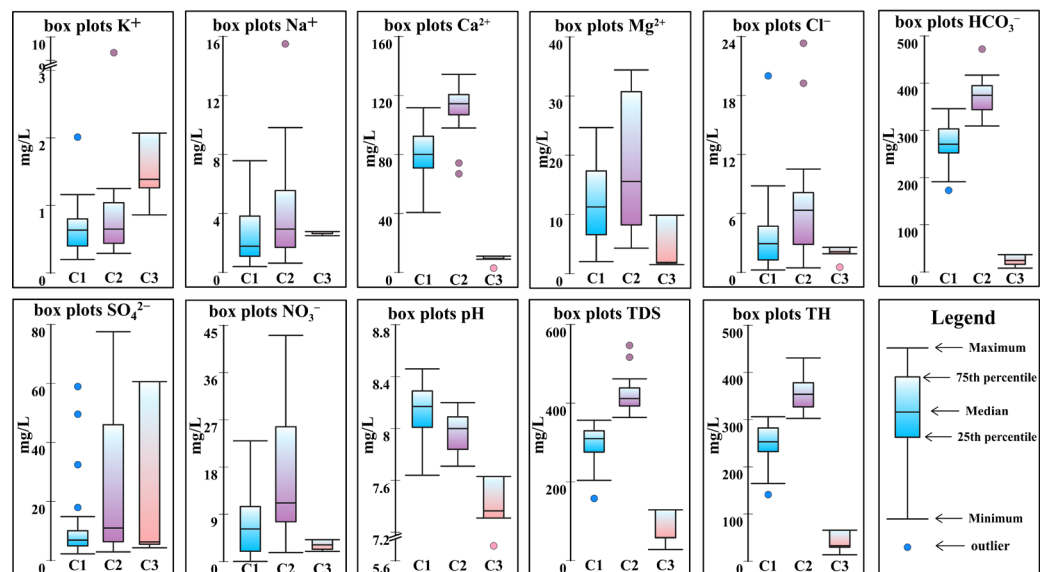


Figure 3. Box plots of groundwater chemical compositions in northeastern Chongqing municipality.

The number of G1 groundwater samples was 30. The pH values ranged from 7.64 to 8.46, with an average of 8.14, emphasizing a weakly alkaline nature. TDS is a crucial parameter in water chemistry analysis [42]. The values ranged from 158 to 357 $mg \cdot L^{-1}$, with an average of 296 $mg \cdot L^{-1}$, and were categorized as freshwater. The TH was typically proportional to the TDS and ranged from 141.15 to 306.26 $mg \cdot L^{-1}$, with a mean of 248.20 $mg \cdot L^{-1}$. The bulk of the samples were moderately hard water (150–300 $mg \cdot L^{-1}$) and hard water (300–450 $mg \cdot L^{-1}$). The cations principally included Ca^{2+} and Mg^{2+} , followed by Na^+ and K^+ . The concentration of Ca^{2+} ranged from 40.63 to 111.68 $mg \cdot L^{-1}$, with a mean of 79.95 $mg \cdot L^{-1}$. The concentration of Mg^{2+} ranged from 2.02 to 24.68 $mg \cdot L^{-1}$, with a mean of 11.72 $mg \cdot L^{-1}$. In addition, anions mainly

included HCO_3^- , followed by SO_4^{2-} and NO_3^- . The concentration of HCO_3^- ranged from 172.98 to 345.95 $\text{mg}\cdot\text{L}^{-1}$, with a mean of 272.42 $\text{mg}\cdot\text{L}^{-1}$. The concentrations of SO_4^{2-} and NO_3^- ranged from 2.27 to 58.99 and 0.0027 to 22.99 $\text{mg}\cdot\text{L}^{-1}$, with means of 11.05 and 6.94 $\text{mg}\cdot\text{L}^{-1}$, respectively. The order of cation components followed the order of $\text{Ca}^{2+} > \text{Mg}^{2+} > \text{Na}^+ > \text{K}^+$, while the anionic components ranked as $\text{HCO}_3^- > \text{SO}_4^{2-} > \text{NO}_3^- > \text{Cl}^-$. The major anions and cations in G1 samples were Ca^{2+} and HCO_3^- , indicative of the Ca- HCO_3 hydrochemical type (Figure 5).

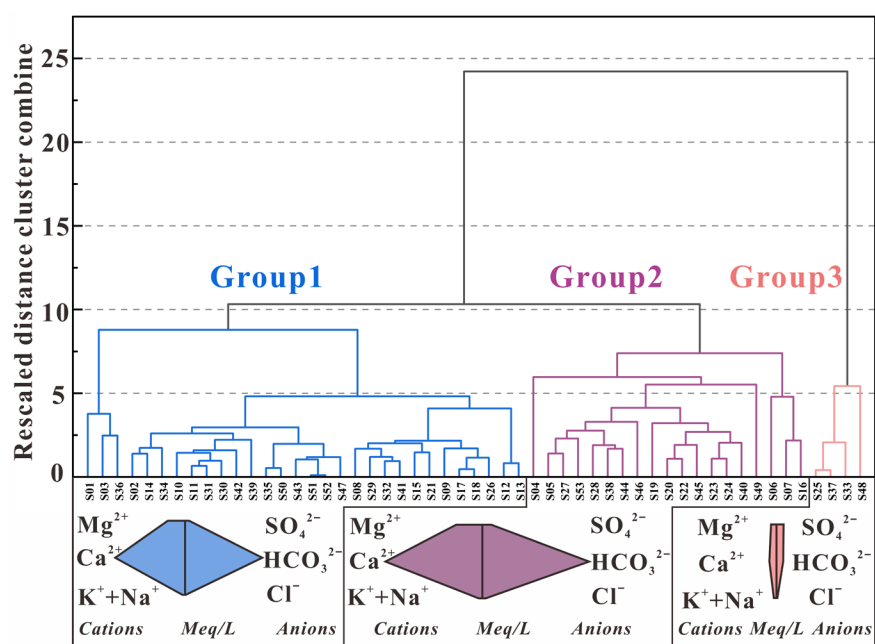


Figure 4. The dendrogram is used to depict the classification of water samples, while major ion concentrations are illustrated with the stiff diagram.

Table 1. Characteristics of diverse chemical indicators in the groundwater of northeastern Chongqing municipality, China.

| Indicator | Maximum | Minimum | Mean | Standard Deviation | Coefficient of Variation (%) | Standard | Rate (%) |
|--------------------|---------|---------|--------|--------------------|------------------------------|----------|----------|
| pH | 8.46 | 5.76 | 7.99 | 0.39 | 5 | 6.5–8.5 | 0 |
| TDS | 547 | 28 | 323.96 | 103.89 | 32 | 1000 | 0 |
| TH | 430.74 | 13.54 | 270.26 | 90.89 | 34 | 450 | 0 |
| EC | 1094 | 116 | 659.31 | 192.71 | 29 | - | - |
| K^+ | 9.33 | 0.2 | 0.90 | 1.23 | 137 | - | - |
| Na^+ | 15.49 | 0.4 | 3.15 | 2.71 | 86 | 200 | 0 |
| Ca^{2+} | 134.3 | 2.92 | 85.95 | 30.95 | 36 | 200 | 0 |
| Mg^{2+} | 34.42 | 1.52 | 13.43 | 9.11 | 68 | 50 | 0 |
| Cl^- | 23.31 | 0.25 | 4.57 | 4.81 | 105 | 250 | 0 |
| HCO_3^- | 472.12 | 36.7 | 290.86 | 97.94 | 34 | - | - |
| SO_4^{2-} | 77.57 | 2.27 | 16.55 | 19.34 | 117 | 250 | 0 |
| NO_3^- | 43.1 | 0.0027 | 10.09 | 10.09 | 100 | 20 | 17 |

Notes: pH has no dimension, EC unit is $\mu\text{s}/\text{cm}$, TH- NO_3^- unit is mg/L ; the standard (STD) derived from Chinese standard for groundwater quality [31] and World Health Organization [41]; rate is the proportion that exceeds the standard level.

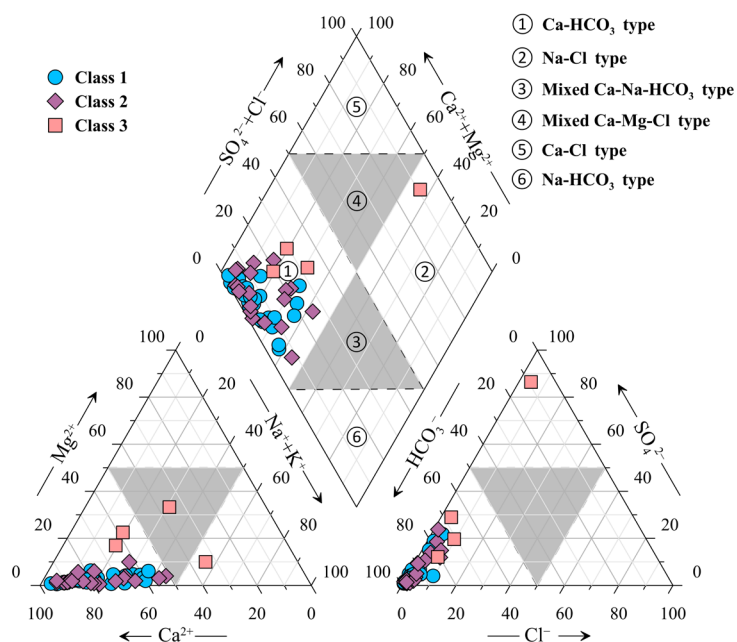


Figure 5. The hydrochemical types of the three groups (G1, G2, and G3) of groundwater in northeastern Chongqing were determined using a Piper trilinear diagram [43].

The number of G2 groundwater samples was 19. The pH values ranged between 7.71 and 8.20, with an average of 7.96, and paralleled those of G1. G2 had the highest TDS values, which ranged from 364 to 547 mg·L⁻¹, with an average of 422 mg·L⁻¹, and was classified as freshwater. Analogous to G1, the TH ranged from 302.61 to 430.74 mg·L⁻¹, with a mean of 354.37 mg·L⁻¹. The cations principally included Ca²⁺ and Mg²⁺, followed by Na⁺ and K⁺. The anions mainly included HCO₃⁻, followed by SO₄²⁻ and NO₃⁻. The distributions of Na⁺ and Cl⁻ were approximated, ranging from 0.63 to 15.49 and 0.46 to 23.31 mg·L⁻¹, with means of 4.21 and 6.93 mg·L⁻¹. Furthermore, the concentrations of Ca²⁺ and HCO₃⁻ ranged from 66.88 to 134.30 and 309.32 to 472.12 mg·L⁻¹, with means of 111.79 and 376.26 mg·L⁻¹. The order of cation components followed the order of Ca²⁺ > Mg²⁺ > Na⁺ > K⁺, while the anionic components ranked as HCO₃⁻ > SO₄²⁻ > NO₃⁻ > Cl⁻. The major anion and cation in G2 samples were Ca²⁺ and HCO₃⁻, indicative of the Ca-HCO₃ hydrochemical type (Figure 5).

The number of G3 samples was four. The pH values ranged from 7.63 to 5.76, with an average of 7.03. These samples had the lowest TDS values (28–129 mg·L⁻¹, with an average of 69 mg·L⁻¹) and were classified as freshwater. The TH ranged from 13.54 to 65.63 mg·L⁻¹, with a mean of 36.20 mg·L⁻¹, indicating extremely soft water throughout (TH < 75 mg·L⁻¹). The cations principally included Ca²⁺, followed by Mg²⁺. The anions principally comprised HCO₃⁻, followed by SO₄²⁻. The concentration of Ca²⁺ ranged from 2.92 to 11.04 mg·L⁻¹, with a mean of 8.23 mg·L⁻¹. The concentration of HCO₃⁻ ranged from 8.14 to 36.70 mg·L⁻¹, with a mean of 23.42 mg·L⁻¹. The order of cation components followed the order of Ca²⁺ > Mg²⁺ > Na⁺ > K⁺, while the anionic components ranked as HCO₃⁻ > SO₄²⁻ > NO₃⁻ > Cl⁻. The major anion and cation in G2 samples were Ca²⁺ and HCO₃⁻, indicative of Ca-HCO₃, Ca-Mg-SO₄, and Ca-Mg-Na-SO₄-HCO₃ hydrochemical types (Figure 5).

In summary, G1 groundwater samples accounted for 56.6% in total, followed by 35.85% for G2, and only 7.55% for G3. It is noted that the TDS and TH concentrations followed the order of G2 > G1 > G3. The higher TDS and TH concentrations were produced by longer flowing times and paths. The differences in the hydrochemical components of the three types of groundwater were mainly caused by different hydrogeochemical processes.

5. Discussion

5.1. Main Factors Dominating Hydrochemistry

The hierarchical cluster analysis showed that the groundwater was controlled by different effects in the study area. Among them, G1 and G2 groundwater samples exhibited higher TDS concentrations, with G2 showing the highest concentrations of NO_3^- and Cl^- . G3 samples, on the other hand, had the shortest runoff path and lower concentrations of various ions. However, the pivotal drivers behind the hydrochemical and geochemical variations within the region remain unclear, requiring further discussion.

5.1.1. Correlations between Hydrochemical Parameters

To investigate the relationship between each parameter and reduce the computational complexity, correlation analysis and PCA were combined to analyze the raw groundwater sample data [44]. The TDS and TH were typically regulated by major ions present in the groundwater, resulting in strong correlations between these parameters and major ions (Ca^{2+} and HCO_3^-) (Figure 6a) [45]. The high correlation coefficient between Ca^{2+} and HCO_3^- (0.934) suggests that they may be controlled by carbonate minerals.

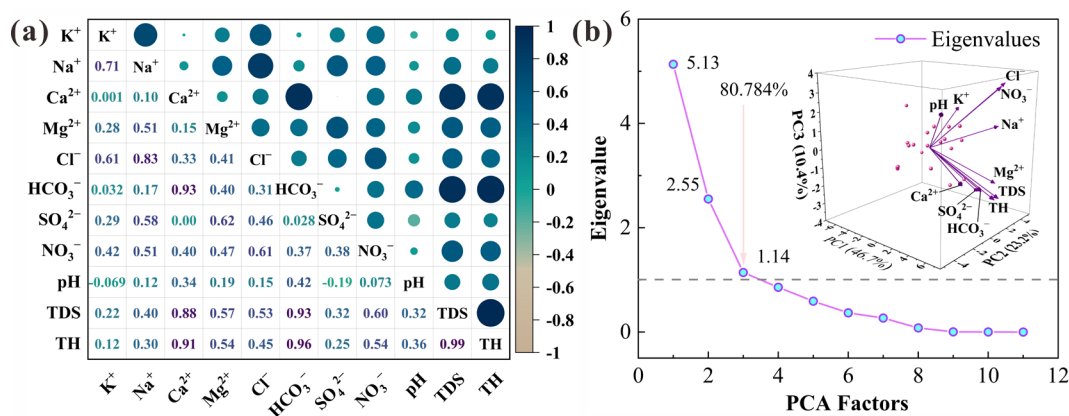


Figure 6. (a) Correlation analysis is primarily used to investigate the interrelationships and mutual influences among different parameters, aiming to ascertain whether there are associations or correlations between them. (b) The Scree plot illustrates the eigenvalues and cumulative variance, while the biplot (3D) depicts the relationships between various indicators.

PCA aims to decrease the dimensionality of multivariate data by extracting complex information and transforming it into a simplified dataset, thereby revealing the underlying structure of the original data [46]. The Kaiser–Meyer–Olkin (KMO) test is a method to assess the statistical significance of a dataset, and a value above 0.5 indicates acceptability, which helps determine the suitability of the research for PCA [47]. The KMO value (0.65) in this study suggested the PCA conclusions were statistically meaningful [48]. The eigenvalues and cumulative variances in PCA provide pivotal information about the data structure and distribution. Based on the Kaiser rule, principal components (PCs) with eigenvalues of greater than one can be retained, which helps to determine the number of PCs to achieve the purpose of data dimensionality reduction [49]. In this research, eigenvalues exceeding 1 were observed for three PCs (5.13, 2.55, and 1.14), which represented 80.784% of the variance (Table 2) (Figure 6b). Regarding the loading values, a value above 7.5 is considered strong, 5–7.5 is moderate, and 0.3–0.5 is weak [50]. PC1 accounted for 48.462% and exhibited strong loadings of Ca (0.746), Cl (0.729), HCO_3^- (0.802), TDS (0.947), and TH (0.91), suggesting significant influences from natural processes such as mineral dissolution and precipitation (carbonate, silicate, or evaporite). Moreover, the notably positive NO_3^- load (0.717) indicated the elevated NO_3^- concentration in the study area. PC2 (23.072%) displayed relatively high loadings of Na (0.646) and K (0.633), highlighting that they have similar sources. The lower loadings of PC3 (9.25%) were attributed to the limited contribution of

this subset of samples to hydrochemical evolution, primarily because of their shorter flow path and the weaker geochemical interactions with the surrounding rock.

Table 2. Matrix of components for principal component analysis; each column contains the loading values for different indices, and the bold values indicate that the values are higher.

| Variable Factor | PC1 | PC2 | PC3 |
|------------------|--------------|--------------|--------|
| Cumulative (%) | 48.462 | 23.072 | 9.250 |
| K | 0.426 | 0.633 | 0.426 |
| Na | 0.64 | 0.646 | 0.23 |
| Ca | 0.746 | −0.584 | 0.064 |
| Mg | 0.666 | 0.272 | −0.424 |
| Cl | 0.729 | 0.455 | 0.301 |
| HCO ₃ | 0.802 | −0.561 | −0.016 |
| SO ₄ | 0.46 | 0.583 | −0.545 |
| NO ₃ | 0.717 | 0.242 | 0.016 |
| pH | 0.339 | −0.397 | 0.432 |
| TDS | 0.947 | −0.28 | −0.102 |
| TH | 0.91 | −0.386 | −0.12 |

5.1.2. Ion Ratio Analysis

In the analysis of the groundwater's chemical evolution, different ion ratios served as valuable indicators to enhance our understanding of the groundwater. The Gibbs diagrams were instrumental in deciding the geochemical processes affecting the groundwater composition, and the end-member diagrams assisted in determining the types of water–rock interactions, while other ion ratios helped clarify the principal sources of ions [17].

Three primary mechanisms govern the processes that hydrochemical components of groundwater undergo, as classified using Gibbs diagrams: precipitation, water–rock interactions, and evaporation [51]. Water–rock interactions describe chemical exchanges between groundwater and surrounding rocks, impacting the composition of the groundwater. All samples fell within the zone of water–rock interactions in this study (Figure 7a,b), indicating that the groundwater chemistry was primarily influenced by water–rock interactions and was not significantly affected by atmospheric precipitation or evaporation.

The primary types of water–rock interactions are silicate weathering, mineral evaporation, and carbonate dissolution, which can be determined by the Ca²⁺/Na⁺, and HCO₃[−]/Na⁺, Ca²⁺/Na⁺, and Mg²⁺/Na⁺ ratios [52]. The G1 and G2 samples were closer to the carbonate dissolution area, indicating that carbonate dissolution dominated the water–rock interactions (Figure 7c,d). Additionally, G3 samples were closer to the silicate dissolution area, suggesting that silicate weathering dominated the water–rock interactions in G3 samples.

The G1 samples were not concentrated near the cation exchange reaction line, suggesting that the cation exchange reaction was not substantial (Figure 8a). In the Na⁺/Cl[−] ratio analysis, the majority of samples diverged from the $y = x$ line, signifying the improbability of halite dissolution (Figure 9a) [53]. In the Ca²⁺ vs. SO₄^{2−} diagram, the samples fell below the $y = x$ line, illustrating that the higher Ca²⁺ content contradicted the likelihood of gypsum dissolution (Figure 9c) [54]. Furthermore, the Ca²⁺ and HCO₃[−] ratio could serve as an indicator of the origin of carbonate rocks. The points were distributed along the $y = x$ and $y = 2x$ dissolution lines, expressing that the Ca²⁺ and HCO₃[−] primarily originated from calcite dissolution (Figure 9d) [17].

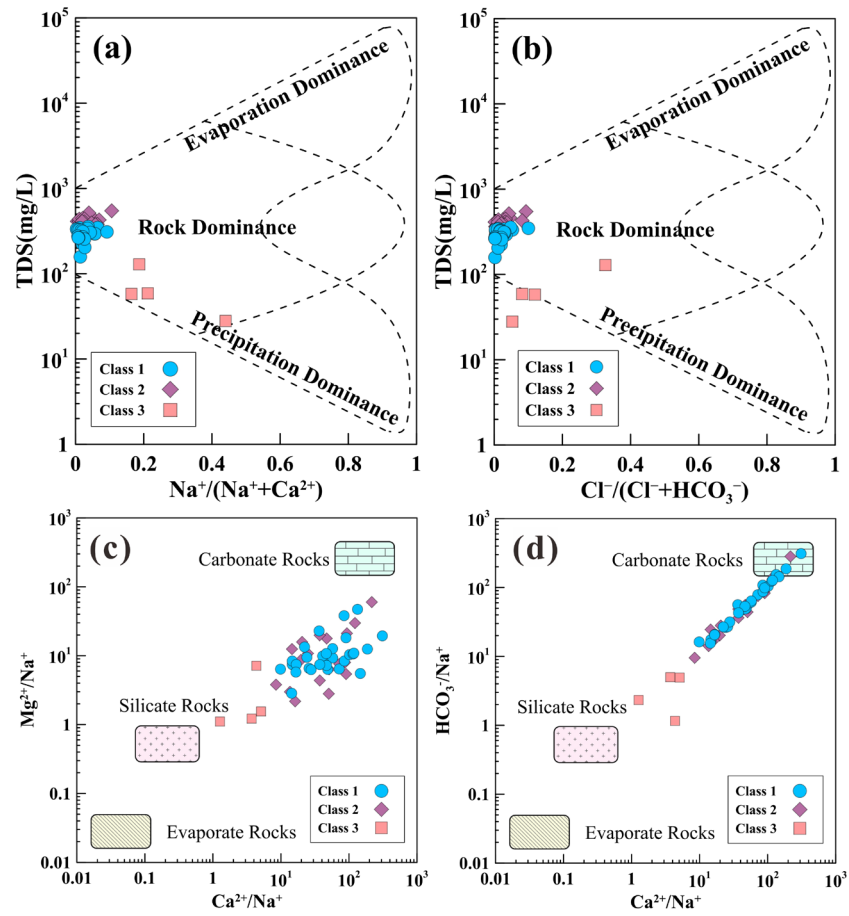


Figure 7. Gibbs distributions and end-member diagrams of groundwater samples. (a) Na⁺/(Na⁺ + Ca²⁺) vs. TDS, (b) Cl⁻/(Cl⁻ + HCO₃⁻) vs. TDS, (c) Ca²⁺/Na⁺ vs. Mg²⁺/Na⁺, and (d) Ca²⁺/Na⁺ vs. HCO₃⁻/Na⁺.

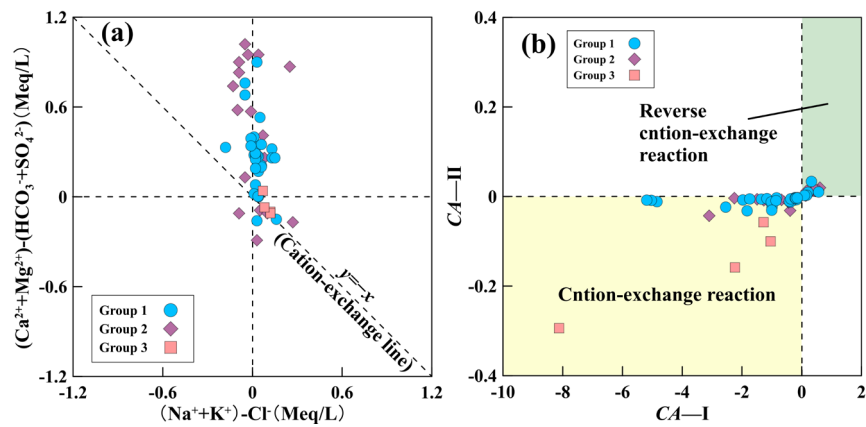


Figure 8. Diagrams of cation exchange reactions. (a) (Na⁺ + K⁺ - Cl⁻) vs. (Ca²⁺ + Mg²⁺ - HCO₃⁻ - SO₄²⁻); (b) CA-I vs. CA-II.

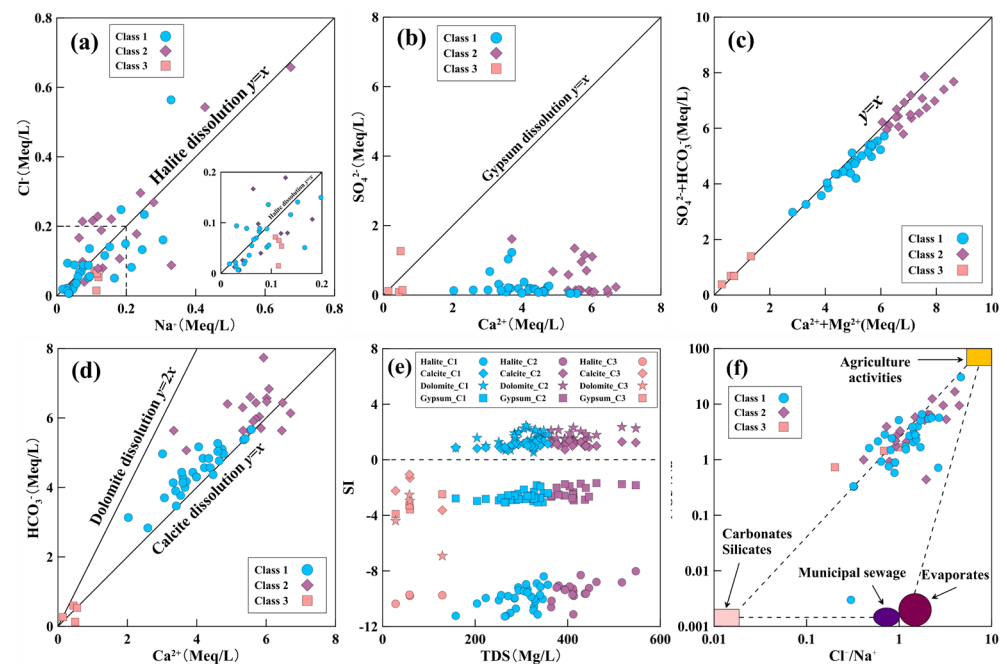


Figure 9. Ion ratio diagrams. (a) Na^+ vs. Cl^- , (b) $\text{Ca}^{2+} + \text{Mg}^{2+}$ vs. $\text{SO}_4^{2-} + \text{HCO}_3^-$, (c) Ca^{2+} vs. SO_4^{2-} , and (d) Ca^{2+} vs. HCO_3^- . (e) Scatter plot of mineral saturation indices and TDS values for groundwater. (f) Cl^-/Na^+ vs. $\text{NO}_3^-/\text{Na}^+$ to determine the NO_3^- pollution sources for groundwater in northeastern Chongqing municipality.

In G2, most of the groundwater samples appeared near the $x = 0$ or $y = 0$ lines, indicating the reaction was insignificant (Figure 8b) [55]. Meanwhile, the rate of Na^+/Cl^- proved that halite dissolution was not the predominant process in G2 samples (Figure 9a). Most of the points (73.7%) fall below the $y = x$ line in Figure 9b, displaying that Ca^{2+} and Mg^{2+} were primarily derived from carbonate mineral dissolution. In the Ca^{2+} vs. HCO_3^- diagram, the G2 samples cluster between the dolomite and calcite dissolution line, providing an explanation for the presence of calcite dissolution (Figure 9d).

In G3 samples, the presence of cation exchange reactions was substantiated by the ratios of $\text{Na}^+ + \text{K}^+ - \text{Cl}^-$ vs. $(\text{Ca}^{2+} + \text{Mg}^{2+}) - (\text{HCO}_3^- + \text{SO}_4^{2-})$ (Figure 8a). CAI-I ($[\text{Cl}^- - (\text{Na}^+ + \text{K}^+)] / \text{Cl}^-$) and CAI-II ($[\text{Cl}^- - (\text{Na}^+ + \text{K}^+)] / [\text{HCO}_3^- + \text{SO}_4^{2-} + \text{CO}_3^{2-} + \text{NO}_3^-]$) values can similarly serve to determine whether ion exchange has occurred in groundwater. Values of greater or less than zero indicate the occurrence of ion exchange; conversely, ion exchange is absent. In G3 samples, the CAI-I and CAI-II values were below zero, hence implying the existence of a cation exchange process (Figure 8b). The G3 samples were spread on the $y = x$ line, illustrating them being predominantly controlled by both carbonate dissolution and silicate weathering (Figure 9c).

To summarize, G1 and G2 groundwater samples were predominantly influenced by the dissolution of calcite minerals. G3 samples displayed evident cation exchange processes and were controlled by silicate weathering. Furthermore, the low ion contents showed that the runoff path of the G3 samples was relatively short, and the water–rock interactions were also limited.

5.1.3. Saturation Indices

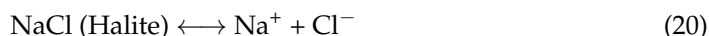
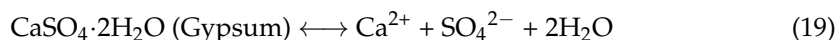
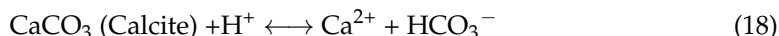
The saturation index (SI) is a geochemical measure indicating whether a solution is oversaturated or undersaturated with respect to specific minerals, which provides vital insights into the potential for mineral precipitation or dissolution in the studied environment. On the other hand, the SI holds significant worth in comprehending the impacts on water quality. The systematic assessment of mineral saturation indices not only aids in the identification of potential water quality issues, such as changes resulting from dissolu-

tion or precipitation processes but also establishes a scientific foundation for sustainable groundwater utilization and management.

The groundwater saturation index (SI) was primarily quantitatively determined through the use of PHREEQC (Figure 9e) [56]. In G1, the SI of calcite and dolomite exceeded 0, ranging from 0.68 to 1.33 and 0.53 to 2.46, with averages of 1.05 and 1.55, manifesting a state of supersaturation (Equations (17) and (18)). Inversely, gypsum and halite had concentrations of less than 0, with saturation coefficients ranging from -3.07 to -1.83 and -11.27 to -8.39 , indicating that both minerals exist in a dissolved state while possessing some dissolution ability (Equations (19) and (20)).

The behavior of G2 samples was consistent with that of G1, where the ranges for calcite and dolomite were 0.73–1.36 and 1.2–2.36, respectively, and for gypsum and halite, the ranges were -2.92 to -1.68 and -11.12 to -8.02 , respectively.

In G3 groundwater samples, the SI values of four minerals were all less than zero. The ranges of values for these coefficients were -3.63 to -1.06 , -6.92 to -2.52 , -3.91 to -2.48 , and -10.36 to -9.71 , demonstrating that the minerals in this type of sample were dissolved while also exhibiting some dissolution ability.



Nitrate (NO_3^-) contamination is influenced by an array of artificial inputs [57]. Most of the points were situated in the upper right corner, illustrating a significant influence of agricultural activities on NO_3^- concentrations in the study area (Figure 9f). This conclusion is consistent with the current predominant use of land by residents.

5.2. Groundwater Suitability for Irrigation

Due to the heavy reliance on agriculture in northeastern Chongqing, appraising groundwater quality for agricultural irrigation purposes is imperative [16]. In general, increased groundwater salinity has a significant impact on soil salinization and crop yields. When hypersaline groundwater is used for irrigation, the soil forms crusts and hardens, thereby inhibiting crop growth [36]. The exchange of sodium ions in groundwater induces a reduction in soil permeability, adversely affecting nutrient absorption by crops [28].

The sodium absorption ratio (SAR) assesses the potential alkalinity hazard to the soil by comparing the concentrations of sodium, calcium, and magnesium in groundwater. Electrical conductivity (EC) is a crucial parameter in groundwater irrigation quality assessment, reflecting groundwater salinity [58]. The calculated SAR ranged from 0.05 to 1.82, with an average value of 0.49. The samples exhibited a range of EC values from 116 to 1094 $\mu\text{S}/\text{cm}$, with an average value of 674.9 $\mu\text{S}/\text{cm}$. The USSL and Wilcox diagrams serve as crucial tools in assessing the suitability of groundwater for irrigation, as they can depict the harmful effects of alkalinity and sodium in groundwater (Figure 10) [28].

The USSL diagram is partitioned into 16 water quality zones based on the appropriateness of the water for irrigation purposes (Figure 10a). Medium and low hazards indicate suitability for most types of soil in groundwater irrigation; a high hazard implies that certain management or treatment is needed before it is suitable for agricultural use; Very a high hazard indicates that the groundwater in this area is not suitable for agricultural irrigation. Table S3 shows the standard EC values. G1 groundwater samples were distributed in areas with medium salinity and low sodium hazards (C2S1), demonstrating that this portion of water is suitable for irrigation purposes on most soil types. G2 groundwater samples (approximately 32.1% of the total) were primarily deployed in regions with high

salinity and low sodium hazards (C3S1). High-salinity groundwater directly affects the absorption of water by plant roots. When soil permeability is feeble, the exchange of water and gas is influenced, leading to crop death [59]. Therefore, these samples were unsuitable for the irrigation of crops grown in poorly drained soils with restricted permeability. G3 samples were predominantly located in the safety zone (C1S1), showing that all water samples from this part of the site are suitable for irrigation purposes.

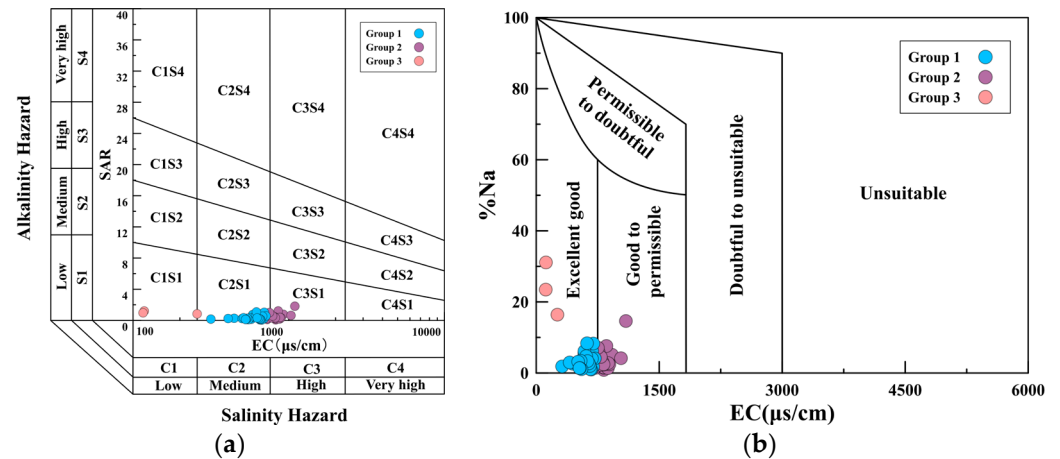


Figure 10. (a) The USSL diagram classifies groundwater samples into 16 categories based on alkalinity and salinity, subsequently determining their suitability for irrigation in the region; (b) the Wilcox diagram illustrates the groundwater irrigation quality based on EC and %Na.

The Wilcox diagram displays that the G1 groundwater samples were principally scattered in an excellent area, while the G2 samples were distributed in a good area (Figure 10b). G3 samples were distributed in an excellent area, but the %Na contents were slightly higher. Based on the correlation between conductivity and sodium content, it can be concluded that there are no irrigation groundwater quality hazards resulting from sodium exchange in the three types of samples within the study area.

The G1 groundwater samples were classified into areas of medium salt hazard and low sodium hazard (C2S1), while G2 samples were situated in regions with high salt hazard and low sodium hazard (C3S1). Hence, the salinity of groundwater should be managed with a focused approach, and sound water conservation facilities can be established to exclude soil salinity using natural water circulation. Measures such as the application of phosphogypsum to filter salts can be implemented if necessary to increase the active calcium cation content in the soil, mitigate crop damage caused by Na_2CO_3 and NaHCO_3 , and lower pH.

5.3. Groundwater Suitability for Drinking

Given that nitrate contamination has been identified in regional hydrogeological mapping and approximately 17% of groundwater samples exceeding 20 mg/L, the EWQI was used to evaluate the suitability of the groundwater quality in the study area.

The EWQI is an efficient technique for the objective appraisal of drinking groundwater quality [17]. The evaluation results ranged from 15 to 94, with a mean value of 73. The groundwater quality varied from excellent (less than 50) to good (50–100). The groundwater quality index and TDS values were predominantly situated within the excellent and good zones (Figure 11a). The G1 and G2 water samples fell within the range of 50–100, while most of the G3 water samples were between 0 and 50. This indicates that the three groups of samples all conform to drinking water specifications.

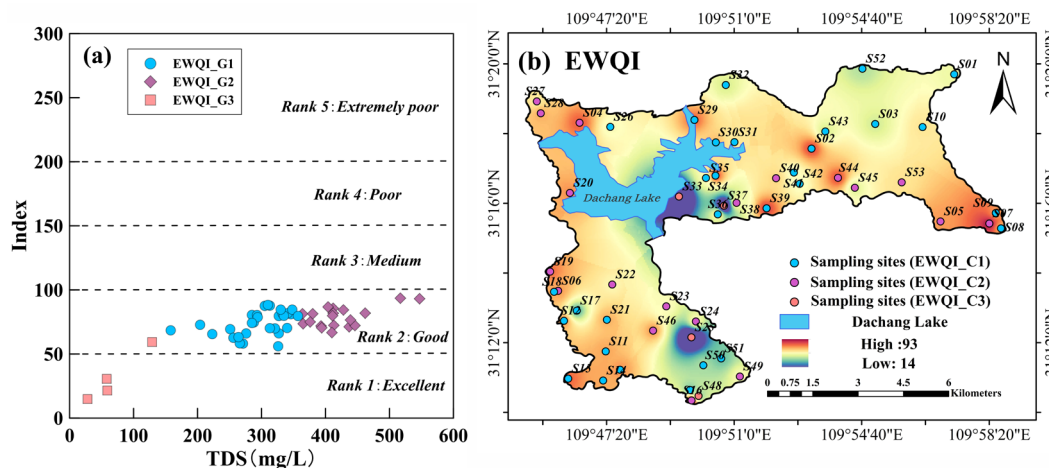


Figure 11. (a) The quality of drinking water is revealed through the use of EWQI and TDS; (b) the distribution of EWQIs among the three groups of samples within the study area.

The EWQI was widely distributed in a patchy pattern with higher water quality in the central region and relatively elevated water quality index values in both the western and eastern regions (Figure 11b). From the sample classification perspective, the G1 and G2 groundwater samples exhibit a more extensive distribution, with most samples located in relatively high EWQI regions, while all G3 samples are allocated in excellent EWQI locations. In a nutshell, the groundwater samples analyzed basically meet drinking water quality standards in this study.

5.4. Non-Carcinogenic Human Health Risks

The objective of this section is to quantify the potential impact of non-carcinogenic pollutants, specifically nitrates, on human health and to explore the sensitivity of different parameters.

Prolonged consumption of nitrate-contaminated groundwater may result in methemoglobinemia, leukemia, gastrointestinal cancer, and other illnesses [60]. Given the widespread distribution of NO_3^- in the area, along with approximately 17% of groundwater samples exceeding the corresponding standard (20 mg/L) for nitrate concentration (Figure 2h; Table 1), there is a potential for adverse effects on three different groups: children (CD), adult females (AFs), and adult males (AMs) [61] (Table S4).

The G1 groundwater samples' nitrate hazard quotient ($\text{HQ}_{\text{Nitrate}}$) values for the three groups had variations of 0.00–1.26 (mean = 0.36), 0.00–0.89 (mean = 0.25), and 0.00–0.76 (mean = 0.21). The G2 samples' $\text{HQ}_{\text{Nitrate}}$ value ranged from 0.06 to 0.67 with a mean of 0.24 for CD, 0.04 to 0.48 with a mean of 0.17 for AF, and 0.03 to 0.40 with a mean of 0.14 for AM. G3 samples' $\text{HQ}_{\text{Nitrate}}$ values ranged from 0.01 to 0.22 with a mean of 0.10 for CD, 0.01 to 0.16 with a mean of 0.07 for AF, and 0.01 to 0.13 with a mean of 0.01 for AM. Among these, only 10% of the G1 samples for CD exceeded one, indicating potential non-carcinogenic health risks related to nitrate. This denotes that CD were at greater risk and were more vulnerable to contaminated groundwater. Additionally, under nitrate contamination, AFs exhibited greater susceptibility compared with AM. To summarize, the analysis ranked the potential health hazards for distinct groups as follows: children > adult females > adult males. This observation stems from the fact that children ingest a greater proportion of water and food relative to their body weight [62].

Spatial distribution maps depicting non-carcinogenic risk levels were generated for different groups (Figure 12). The results of the HHR model reveal that regions with elevated risk for CD were primarily concentrated in the northwestern and eastern areas, but the scope of the high-risk range was limited to 5.66% of the total region. The high-risk range for AM and AF was not detected. Overall, the human health risk was low in most parts of the research region. Local areas with high health risks should be paid attention to with

monitoring techniques. Moreover, the authorities should implement measures such as avoiding excessive use of nitrogen fertilizers, raising awareness of safe water practices among local residents, prioritizing the use of high-quality regional groundwater, and employing targeted water treatment.

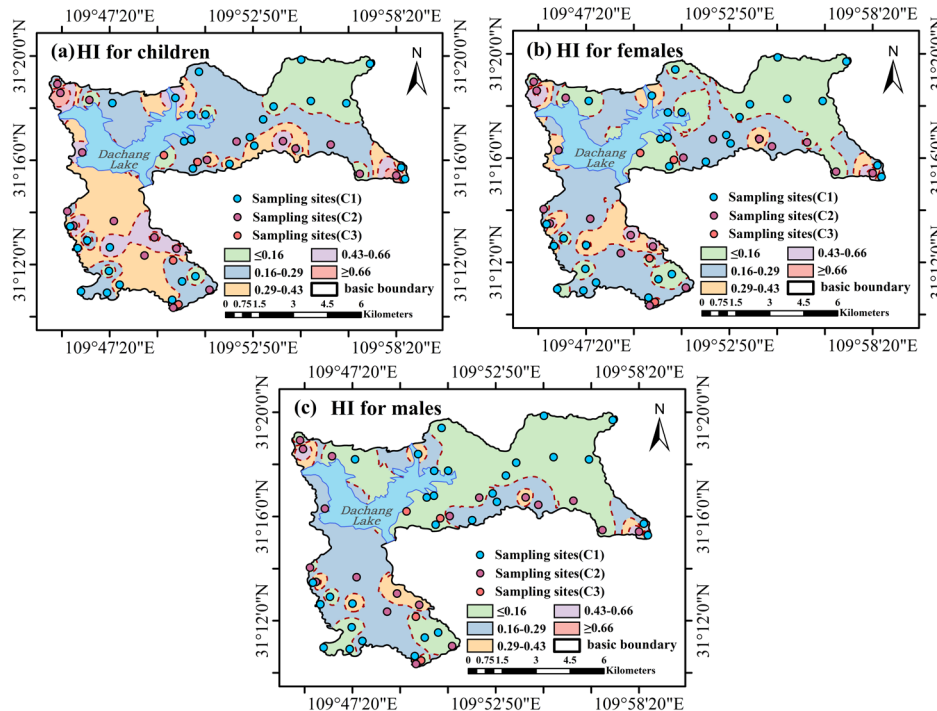


Figure 12. Spatial distribution diagrams of human non-carcinogenic risk assessment for different age groups: (a) children, (b) males, and (c) females.

Sensitivity analysis is a crucial part of the weight of different variables in the HHR model [26]. In this research, specific parameters were chosen for sensitivity analysis, including NO₃, BW, EF, and IR. The sensitivity of these parameters was determined using the Crystal Ball software (version 11.1; Oracle Inc., Austin, TX, USA) (Table 3). The NO₃ concentration exhibited the highest sensitivity, with values of 94.9% in children, 94.2% in adult males, and 93.2% in adult females. This clearly indicates that NO₃ was the primary influencing factor determining the level of human health risk. Consistently, the spatial distribution of high NO₃ concentrations closely resembled the distribution of low EWQIs and high HI values. In comparison, IR and EF demonstrated relatively lower sensitivities, with IR slightly exceeding EF. Negative sensitivity was detected for BW. Many scholars have come to similar conclusions, and the underlying reasons remain to be further studied [63–65]. In terms of the impact order in the sensitivity analysis, a ranking of NO₃ > BW > IR > EF was achieved.

Table 3. Sensitivity variance contributions of three groups to each parameter.

| Parameter | HI_NO ₃ for CD | HI_NO ₃ for AFs | HI_NO ₃ for AMs |
|-----------------|---------------------------|----------------------------|----------------------------|
| BW | −1.8% | −2.8% | −4.5% |
| EF | 0.9% | 0.8% | 0.6% |
| IR | 2.4% | 2.2% | 1.7% |
| NO ₃ | 94.9% | 94.2% | 93.2% |

6. Conclusions

In this paper, 53 groundwater samples were collected from the northern part of Chongqing, SW China. The irrigation suitability using the physicochemical index was

calculated to evaluate its applicability in agricultural activities. Subsequently, the EWQI was computed for groundwater quality evaluation. Eventually, the human health risk assessment model was employed to determine the non-carcinogenic risk of nitrate in groundwater for children, adult females, and adult males. The primary discoveries are outlined as follows:

- (1) Based on the HCA, three classes of groundwater samples were identified in the study region. The groundwater samples overall exhibited predominantly alkaline characteristics, with a predominance of hard water. The cationic components followed the order of $\text{Ca}^{2+} > \text{Mg}^{2+} > \text{Na}^+ > \text{K}^+$, and the anionic components were relatively abundant in the order of $\text{HCO}_3^- > \text{SO}_4^{2-} > \text{NO}_3^- > \text{Cl}^-$. Among them, the hydrochemical types of G1 and G2 samples were mainly identified as Ca-HCO₃, while G3 samples exhibited Ca-HCO₃, Ca-Mg-SO₄, and Ca-Mg-Na-SO₄-HCO₃ types. The composition of groundwater is primarily influenced by water–rock interactions: carbonate dissolution for G1 and G2 samples, and carbonate dissolution and silicate weathering for G3 samples.
- (2) The USSL and Wilcox diagrams revealed that the majority of the groundwater within the study area is deemed suitable for agricultural irrigation. However, 32.1% of the distributed groundwater is situated within high-salinity and low-sodium-hazard zones, signifying that these samples are unsuitable for crops grown in poorly drained soils with restricted permeability. The EWQI values demonstrated that all groundwater samples met the requirements for the basic potable standard.
- (3) Groundwater nitrate contamination was ranked by age and gender as children > adult females > adult males. The sensitivity analysis expressed the NO₃ concentration as exhibiting the highest sensitivity (94.1%) and the influence sequence of each parameter as NO₃ > BW > IR > EF. Long-term use of groundwater in this region should give rise to human health risks (especially in children). Therefore, inhabitants who rely on water in these areas should seek alternative sources to fulfill their needs and mitigate the risks associated with nitrate contamination.
- (4) The salinity of groundwater should be managed with a focused approach by authorities, and sound water conservation facilities can be established to exclude soil salinity using natural water circulation. Moreover, they should implement measures such as avoiding excessive use of nitrogen fertilizers, raising awareness of safe water practices among local residents, and employing targeted water treatment.

Supplementary Materials: The following supporting information can be downloaded at <https://www.mdpi.com/article/10.3390/w15234095/s1>. Table S1: Classification criteria of water quality based on EWQI; Table S2: Parameters for computing the health risks via oral intake and dermal contact exposure pathways; Table S3: Classification of salt hazards in irrigation groundwater; Table S4: Results of non-carcinogenic risk via drinking water intake and dermal contact.

Author Contributions: Methodology, J.L. (Jiawei Liu), C.Y. and J.L. (Junyi Li); Software, Y.W. (Yangshuang Wang), X.Z. and Q.H.; Formal analysis, C.Y. and Y.W. (Yangshuang Wang); Investigation, J.L. (Jiawei Liu), C.Y., S.C., X.Z., W.K., J.L. (Junyi Li) and X.Y.; Resources, W.K.; Data curation, C.Y. and Q.H.; Writing—original draft, J.L. (Jiawei Liu); Writing—review & editing, X.Y.; Supervision, S.C., Y.W. (Ying Wang) and X.Y.; Project administration, S.C.; Funding acquisition, Y.W. (Ying Wang) All authors have read and agreed to the published version of the manuscript.

Funding: This study was funded by the Yibin government (grant number: SWJTU2021020007; SWJTU2021020008), Natural Science Foundation of Chongqing (grant number: cstc2020jcyj-msmX1072; CSTB2022NSCQMSX0881), National Natural Science Foundation of China (grant number: 42072313), Natural Science Foundation of Sichuan Province (grant number: 2022NSFSC0413), the Open Project Program of Engineering Research Center of Groundwater Pollution Control and Remediation, the Ministry of Education of China (grant number: GW202213, GW202308), and the Scientific Key R&D project of the Tibet Autonomous Region (XZ202201ZY0021G).

Data Availability Statement: The data presented in this study are available upon request from the corresponding author.

Acknowledgments: We would like to thank the anonymous reviewers and editors for their constructive comments on this manuscript.

Conflicts of Interest: The authors declare no conflict of interest.

References

- Li, P.; He, X.; Guo, W. Spatial groundwater quality and potential health risks due to nitrate ingestion through drinking water: A case study in Yan'an City on the Loess Plateau of northwest China. *Hum. Ecol. Risk Assess. Int. J.* **2019**, *25*, 11–31. [[CrossRef](#)]
- Liu, M.; Xiao, C.; Liang, X.; Wei, H. Response of groundwater chemical characteristics to land use types and health risk assessment of nitrate in semi-arid areas: A case study of Shuangliao City, Northeast China. *Ecotoxicol. Environ. Saf.* **2022**, *236*, 113473. [[CrossRef](#)]
- Jiang, W.; Sheng, Y.; Liu, H.; Ma, Z.; Song, Y.; Liu, F.; Chen, S. Groundwater quality assessment and hydrogeochemical processes in typical watersheds in Zhangjiakou region, northern China. *Environ. Sci. Pollut. Res. Int.* **2022**, *29*, 3521–3539. [[CrossRef](#)] [[PubMed](#)]
- Ministry of Water Resources the People's Republic of China. *China Water Resources Bulletin 2020*; Ministry of Water Resources, PRC: Beijing, China, 2021. (In Chinese)
- Ministry of Ecology and Environment the People's Republic of China. *Report on the State of the Ecology and Environment in China 2020*; Ministry of Ecology and Environment, PRC: Beijing, China, 2021. (In Chinese)
- Li, Z.; Yang, Q.; Yang, Y.; Xie, C.; Ma, H. Hydrogeochemical controls on arsenic contamination potential and health threat in an intensive agricultural area, northern China. *Environ. Pollut.* **2020**, *256*, 113455. [[CrossRef](#)]
- Fan, A.M.; Steinberg, V.E. Health Implications of Nitrate and Nitrite in Drinking Water: An Update on Methemoglobinemia Occurrence and Reproductive and Developmental Toxicity. *Regul. Toxicol. Pharmacol.* **1996**, *23*, 35–43. [[CrossRef](#)]
- Forman, D.; Al-Dabbagh, S.; Doll, R. Nitrates, nitrites and gastric cancer in Great Britain. *Nature* **1985**, *313*, 620–625. [[CrossRef](#)] [[PubMed](#)]
- Adimalla, N.; Qian, H. Groundwater quality evaluation using water quality index (WQI) for drinking purposes and human health risk (HHR) assessment in an agricultural region of Nanganur, south India. *Ecotoxicol. Environ. Saf.* **2019**, *176*, 153–161. [[CrossRef](#)]
- Saraswat, A.; Ram, S.; Kouadri, S.; Raza, M.B.; Hombegowda, H.C.; Kumar, R.; Golui, D.; Maurya, P.K.; Ilić, P.; Rahman, M.M.; et al. Groundwater quality, fluoride health risk and geochemical modelling for drinking and irrigation water suitability assessment in Tundla block, Uttar Pradesh, India. *Groundw. Sustain. Dev.* **2023**, *23*, 100991. [[CrossRef](#)]
- Ghosh, D.; Mandal, M.; Karmakar, M.; Banerjee, M.; Mandal, D. Application of geospatial technology for delineating groundwater potential zones in the Gandheswari watershed, West Bengal. *Sustain. Water Resour. Manag.* **2020**, *6*, 6–11. [[CrossRef](#)]
- Chowdhury, P.; Mukhopadhyay, B.P.; Bera, A. Hydrochemical assessment of groundwater suitability for irrigation in the northeastern blocks of Purulia district, India using GIS and AHP techniques. *Phys. Chem. Earth Parts A/B/C* **2022**, *126*, 103–108. [[CrossRef](#)]
- Kim, K.-H.; Yun, S.-T.; Yu, S.; Choi, B.-Y.; Kim, M.-J.; Lee, K.-J. Geochemical pattern recognitions of deep thermal groundwater in South Korea using self-organizing map: Identified pathways of geochemical reaction and mixing. *J. Hydrol.* **2020**, *589*, 125202. [[CrossRef](#)]
- Yang, W.; Zhao, Y.; Wang, D.; Wu, H.; Lin, A.; He, L. Using Principal Components Analysis and IDW Interpolation to Determine Spatial and Temporal Changes of Surface Water Quality of Xin'anjiang River in Huangshan, China. *Int. J. Environ. Res. Public Health* **2020**, *17*, 082942. [[CrossRef](#)]
- Daughney, C.J.; Raiber, M.; Moreau-Fournier, M.; Morgenstern, U.; Raaij, R.v.d. Use of hierarchical cluster analysis to assess the representativeness of a baseline groundwater quality monitoring network: Comparison of New Zealand's national and regional groundwater monitoring programs. *Hydrogeol. J.* **2012**, *20*, 185–200. [[CrossRef](#)]
- Zhao, X.; Guo, H.; Wang, Y.; Wang, G.; Wang, H.; Zang, X.; Zhu, J. Groundwater hydrogeochemical characteristics and quality suitability assessment for irrigation and drinking purposes in an agricultural region of the North China plain. *Environ. Earth Sci.* **2021**, *80*, 162. [[CrossRef](#)]
- Zhang, Y.; Dai, Y.; Wang, Y.; Huang, X.; Xiao, Y.; Pei, Q. Hydrochemistry, quality and potential health risk appraisal of nitrate enriched groundwater in the Nanchong area, southwestern China. *Sci. Total Environ.* **2021**, *784*, 147186. [[CrossRef](#)]
- Wang, Y.; Liu, J.; Yu, X.; Yan, Y.; Chen, Q.; Chen, S. Evaluation of groundwater quality and health risk assessment in southeastern Tibet, China. *Environ. Earth Sci.* **2023**, *82*, 455. [[CrossRef](#)]
- Chen, S.; Tang, Z.; Wang, J.; Wu, J.; Yang, C.; Kang, W.; Huang, X. Multivariate Analysis and Geochemical Signatures of Shallow Groundwater in the Main Urban Area of Chongqing, Southwestern China. *Water* **2020**, *12*, 2833. [[CrossRef](#)]
- NBS; PRC. *2020 China Statistical Yearbook*; China Statistical Press: Beijing, China, 2020. (In Chinese)
- Pu, J.; Yuan, D.; Xiao, Q.; Zhao, H. Hydrogeochemical characteristics in karst subterranean streams: A case history from Chongqing, China. *Carbonates Evaporites* **2015**, *30*, 307–319. [[CrossRef](#)]
- Zheng, D.; Liu, Y.; Luo, L.; Shahid, M.Z.; Hou, D. Spatial variation and health risk assessment of fluoride in drinking water in the Chongqing urban areas, China. *Environ. Geochem. Health* **2020**, *42*, 2925–2941. [[CrossRef](#)] [[PubMed](#)]

23. Yang, X.; Fu, J.; Han, X.; Zhang, C.; Pan, S.; Li, G.; Guo, Y.; Pan, J. Progress of geological hazards survey in the urban area from Wanzhou to Wushan in Three Gorges Reservoir. *Geol. Surv. China* **2021**, *8*, 97–107.
24. Pu, J.; Yuan, D.; Zhang, C.; Zhao, H. Hydrogeochemistry and possible sulfate sources in karst groundwater in Chongqing, China. *Environ. Earth Sci.* **2012**, *68*, 159–168. [[CrossRef](#)]
25. Yang, F.; Jia, C.; Yang, X.; Yang, H.; Chang, W. Probabilistic potential health risk quantification, hydrochemistry, driving forces of groundwater nitrate and fluoride in a typical irrigation district, Northern China. *J. Environ. Manag.* **2022**, *323*, 116171. [[CrossRef](#)] [[PubMed](#)]
26. Eldaw, E.; Huang, T.; Mohamed, A.K.; Mahama, Y. Classification of groundwater suitability for irrigation purposes using a comprehensive approach based on the AHP and GIS techniques in North Kurdufan Province, Sudan. *Appl. Water Sci.* **2021**, *11*, 126. [[CrossRef](#)]
27. Singh, A.K.; Tewary, B.K.; Sinha, A. Hydrochemistry and quality assessment of groundwater in part of Noida metropolitan city, Uttar Pradesh. *J. Geol. Soc. India* **2011**, *78*, 523–540. [[CrossRef](#)]
28. Bian, J.; Nie, S.; Wang, R.; Wan, H.; Liu, C. Hydrochemical characteristics and quality assessment of groundwater for irrigation use in central and eastern Songnen Plain, Northeast China. *Environ. Monit. Assess.* **2018**, *190*, 382. [[CrossRef](#)]
29. Gautam, U.; Tiwari, V.; Tripathi, V.K. Evaluation of groundwater quality of Prayagraj city using entropy water quality index (EWQI) and new integrated water quality index (IWQI). *Sustain. Water Resour. Manag.* **2022**, *8*, 57. [[CrossRef](#)]
30. Li, P.-Y.; Qian, H.; Wu, J.-H. Groundwater Quality Assessment Based on Improved Water Quality Index in Pengyang County, Ningxia, Northwest China. *E-J. Chem.* **2010**, *7*, S209–S216.
31. GB/T 14848-2017; GAQS (General Administration of Quality Supervision) and SAC (Standardization Administration of China): Standard for Groundwater Quality. Standardization Administration of the PRC: Beijing, China, 2017.
32. Li, X.; Huang, X.; Zhang, Y. Spatio-temporal analysis of groundwater chemistry, quality and potential human health risks in the Pinggu basin of North China Plain: Evidence from high-resolution monitoring dataset of 2015–2017. *Sci. Total Environ.* **2021**, *800*, 149568. [[CrossRef](#)]
33. Wang, Y.; Li, P. Appraisal of shallow groundwater quality with human health risk assessment in different seasons in rural areas of the Guanzhong Plain (China). *Environ. Res.* **2022**, *207*, 112210. [[CrossRef](#)]
34. Yuan, Y.; Liu, Y.; Luo, K.; Shahid, M.Z. Hydrochemical characteristics and a health risk assessment of the use of river water and groundwater as drinking sources in a rural area in Jiangjin District, China. *Environ. Earth Sci.* **2020**, *79*, 160. [[CrossRef](#)]
35. Li, Y.; Li, P.; Cui, X.; He, S. Groundwater quality, health risk, and major influencing factors in the lower Beiluo River watershed of northwest China. *Hum. Ecol. Risk Assess. Int. J.* **2021**, *27*, 1987–2013. [[CrossRef](#)]
36. Liu, J.; Gao, Z.; Wang, Z.; Xu, X.; Su, Q.; Wang, S.; Qu, W.; Xing, T. Hydrogeochemical processes and suitability assessment of groundwater in the Jiaodong Peninsula, China. *Environ. Monit. Assess.* **2020**, *192*, 384. [[CrossRef](#)] [[PubMed](#)]
37. Sharma, T.; Bajwa, B.S.; Kaur, I. Hydro-geochemical characteristics and quality appraisal of aquifers using multivariate statistics and associated risk assessment in Tarn-Taran district, Punjab, India. *Environ. Sci. Pollut. Res. Int.* **2022**, *29*, 54916–54938. [[CrossRef](#)]
38. Güler, C.; Thyne, G.D. Hydrologic and geologic factors controlling surface and groundwater chemistry in Indian Wells-Owens Valley area, southeastern California, USA. *J. Hydrol.* **2004**, *285*, 177–198. [[CrossRef](#)]
39. Wu, J.; Li, P.; Wang, D.; Ren, X.; Wei, M. Statistical and multivariate statistical techniques to trace the sources and affecting factors of groundwater pollution in a rapidly growing city on the Chinese Loess Plateau. *Hum. Ecol. Risk Assess. Int. J.* **2019**, *26*, 1603–1621. [[CrossRef](#)]
40. Feng, F.; Jia, Y.; Yang, Y.; Huan, H.; Lian, X.; Xu, X.; Xia, F.; Han, X.; Jiang, Y. Hydrogeochemical and statistical analysis of high fluoride groundwater in northern China. *Environ. Sci. Pollut. Res. Int.* **2020**, *27*, 34840–34861. [[CrossRef](#)] [[PubMed](#)]
41. WHO. *Guidelines for Drinking-Water Quality*, 4th ed.; World Health Organization: Geneva, Switzerland, 2017.
42. Geng, J.; Chen, J.; Zhang, S. Analysis of Hydro-Chemical Changes and Genesis of Major Ions in Upper Reach of Chishui River. *Juornal China Hydrol.* **2013**, *33*, 44–50.
43. Piper, A.M. A graphical procedure in the geochemical interpretation of water analysis. *Eos Trans. Am. Geophys. Union* **1944**, *25*, 914–928.
44. Dashora, M.; Kumar, A.; Kumar, S.; Kumar, P.; Kumar, A.; Singh, C.K. Geochemical assessment of groundwater in a desertic region of India using chemometric analysis and entropy water quality index (EWQI). *Nat. Hazards* **2022**, *112*, 747–782. [[CrossRef](#)]
45. Wu, H.; Xu, C.; Wang, J.; Xiang, Y.; Ren, M.; Qie, H.; Zhang, Y.; Yao, R.; Li, L.; Lin, A. Health risk assessment based on source identification of heavy metals: A case study of Beiyun River, China. *Ecotoxicol. Environ. Saf.* **2021**, *213*, 112046. [[CrossRef](#)]
46. Swain, S.; Sahoo, S.; Taloor, A.K. Groundwater quality assessment using geospatial and statistical approaches over Faridabad and Gurgaon districts of National Capital Region, India. *Appl. Water Sci.* **2022**, *12*, 75. [[CrossRef](#)]
47. Kaiser, H.F. An index of factorial simplicity. *Psychometrika* **1974**, *39*, 31–36. [[CrossRef](#)]
48. Zhang, H.; Cheng, S.; Li, H.; Fu, K.; Xu, Y. Groundwater pollution source identification and apportionment using PMF and PCA-APCA-MLR receptor models in a typical mixed land-use area in Southwestern China. *Sci. Total Environ.* **2020**, *741*, 140383. [[CrossRef](#)] [[PubMed](#)]
49. Gholizadeh, H.M.; Melesse, A.M.; Reddi, L. Water quality assessment and apportionment of pollution sources using APCS-MLR and PMF receptor modeling techniques in three major rivers of South Florida. *Sci. Total Environ.* **2016**, *566–567*, 1552–1567. [[CrossRef](#)] [[PubMed](#)]

50. Liu, C.W.; Lin, K.H.; Kuo, Y.M. Application of factor analysis in the assessment of groundwater quality in a blackfoot disease area in Taiwan. *Sci. Total Environ.* **2003**, *313*, 77–89. [[CrossRef](#)]
51. Gibbs, R.J. Mechanisms Controlling World Water Chemistry. *Science* **1970**, *170*, 1088–1090. [[CrossRef](#)]
52. Gaillardet, J.; Dupré, B.; Louvat, P.; Allègre, C. Global silicate weathering and CO₂ consumption rates deduced from the chemistry of large rivers. *Chem. Geol.* **1999**, *159*, 3–30. [[CrossRef](#)]
53. Wu, C.; Wu, X.; Qian, C.; Zhu, G. Hydrogeochemistry and groundwater quality assessment of high fluoride levels in the Yanchi endorheic region, northwest China. *Appl. Geochem.* **2018**, *98*, 404–417. [[CrossRef](#)]
54. Lv, G.; Zhang, X.; Wei, D.; Yu, Z.; Yuan, X.; Sun, M.; Kong, X.; Zhang, Y. Water–Rock Interactions, Genesis Mechanism, and Mineral Scaling of Geothermal Waters in Northwestern Sichuan, SW China. *Water* **2023**, *15*, 3730. [[CrossRef](#)]
55. Wang, Y.; Yuan, X.; Zhang, Y.; Zhang, X.; Xiao, Y.; Duo, J.; Huang, X.; Sun, M.; Lv, G. Hydrochemical, D–O–Sr isotopic and electromagnetic characteristics of geothermal waters from the Erdaoqiao area, SW China: Insights into genetic mechanism and scaling potential. *Ore Geol. Rev.* **2023**, *158*, 105486. [[CrossRef](#)]
56. Chen, K.; Liu, Q.; Yang, T.; Ju, Q.; Hou, X.; Gao, W.; Jiang, S. Groundwater pollution source identification and health risk assessment in the North Anhui Plain, eastern China: Insights from positive matrix factorization and Monte Carlo simulation. *Sci. Total Environ.* **2023**, *895*, 165186. [[CrossRef](#)]
57. Adimalla, N. Application of the Entropy Weighted Water Quality Index (EWQI) and the Pollution Index of Groundwater (PIG) to Assess Groundwater Quality for Drinking Purposes: A Case Study in a Rural Area of Telangana State, India. *Arch. Environ. Contam. Toxicol.* **2021**, *80*, 31–40. [[CrossRef](#)]
58. Richards, L.A. Diagnosis and Improvement of Saline and Alkali Soils. *Agric. Handb.* **1954**, *60*, 129–134. [[CrossRef](#)]
59. Oster, J.D.; Shainberg, I. Soil responses to sodicity and salinity: Challenges and opportunities. *Soil Res.* **2001**, *39*, 1219. [[CrossRef](#)]
60. Liu, Y.; Sheng, Y.; Feng, C.; Chen, N.; Liu, T. Distinct functional microbial communities mediating the heterotrophic denitrification in response to the excessive Fe (II) stress in groundwater under wheat-rice stone and rock phosphate amendments. *Environ. Res.* **2020**, *185*, 109391. [[CrossRef](#)] [[PubMed](#)]
61. Ju, Q.; Hu, Y.; Liu, Q.; Chai, H.; Chen, K.; Zhang, H.; Wu, Y. Source apportionment and ecological health risks assessment from major ions, metalloids and trace elements in multi-aquifer groundwater near the Sunan mine area, Eastern China. *Sci. Total Environ.* **2023**, *860*, 160454. [[CrossRef](#)] [[PubMed](#)]
62. Zhang, Y.; Li, X.; Luo, M.; Wei, C.; Huang, X.; Xiao, Y.; Qin, L.; Pei, Q.; Gao, X. Hydrochemistry and Entropy-Based Groundwater Quality Assessment in the Suining Area, Southwestern China. *J. Chem.* **2021**, *2021*, 5591892. [[CrossRef](#)]
63. Mukherjee, I.; Singh, U.K.; Singh, R.P.; Anshumali; Kumari, D.; Jha, P.K.; Mehta, P. Characterization of heavy metal pollution in an anthropogenically and geologically influenced semi-arid region of east India and assessment of ecological and human health risks. *Sci. Total Environ.* **2020**, *705*, 135801. [[CrossRef](#)]
64. Gao, B.; Gao, L.; Gao, J.; Xu, D.; Wang, Q.; Sun, K. Simultaneous evaluations of occurrence and probabilistic human health risk associated with trace elements in typical drinking water sources from major river basins in China. *Sci. Total Environ.* **2019**, *666*, 139–146. [[CrossRef](#)]
65. Meng, Y.; Wu, J.; Li, P. Distribution characteristics, source identification and health risk assessment of trace metals in the coastal groundwater of Taizhou City, China. *Environ. Res.* **2023**, *238*, 117085. [[CrossRef](#)]

Disclaimer/Publisher’s Note: The statements, opinions and data contained in all publications are solely those of the individual author(s) and contributor(s) and not of MDPI and/or the editor(s). MDPI and/or the editor(s) disclaim responsibility for any injury to people or property resulting from any ideas, methods, instructions or products referred to in the content.